Low-energy electron diffraction study of incommensurate H₂, HD, and D₂ monolayers physisorbed on graphite

Jinhe Cui* and Samuel C. Fain, Jr.

Department of Physics (FM-15), University of Washington, Seattle, Washington 98195

(Received 6 July 1988)

Incommensurate (IC) monolayer phases of H_2, HD, and D_2 physisorbed on graphite single crystals are studied by low-energy electron diffraction (LEED). At temperatures near 5 K, a uniaxial IC (UIC) phase and a higher-density rotated IC (RIC) triangular solid phase are observed for monolayers of H_2, HD, and D_2. The commensurate (C) to UIC phase transition of the H_2 monolayer is examined by measuring two-dimensional intensity contours of LEED spots at densities 1.0–1.09 times the C $(\sqrt{3} \times \sqrt{3})R30°$ phase density. The orientation angles of the RIC phase approximately agree with the prediction of Novaco and McTague's calculation for a weakly modulated two-dimensional Cauchy solid. The γ phase, which was first observed in heat-capacity measurements for D_2 on graphite, has been determined to be an IC triangular rotated phase with rotation angle greater than that of the higher-density RIC phase. LEED data from the oriented fluid phases are also presented. A phase diagram for D_2 is proposed based on LEED, heat-capacity, and neutron-diffraction measurements.

I. INTRODUCTION

The study of the physisorption of H_2 and its isotopes HD and D_2 on the graphite surface has been a subject of interesting experimental and theoretical research.[1-10] Analogous to physisorbed systems such as Kr on graphite[11] and Xe on Pt(111),[12] H_2, HD, and D_2 monolayers form a commensurate (C) $(\sqrt{3} \times \sqrt{3})R 30°$ phase at submonolayer coverages and an incommensurate (IC) triangular phase at coverages near monolayer completion.[1] In addition, several intermediate IC phases are also observed by heat-capacity measurements at coverages between the C phase and the IC triangular phase.[3-6] The study of these IC phases provides a realization of effects caused by competition between adsorbate-adsorbate and adsorbate-substrate interactions.

The structures of IC H_2, HD, and D_2 monolayers were first probed by elastic neutron diffraction for H_2 and D_2 and inelastic neutron scattering for HD.[1] The structure deduced from the neutron data is a uniformly compressed IC phase with a triangular unit mesh. Neither the structure of the intermediate IC phases nor the orientation of the IC phases relative to the C-phase direction were determined due to the powder nature of the exfoliated graphite (Grafoil) substrate and the interference of the bulk graphite (002) reflection. Unlike neutron diffraction, where exfoliated graphite has to be used due to the weak scattering signal, low-energy electron diffraction (LEED) uses a graphite single crystal and can thus probe the two-dimensional reciprocal space of the adsorbed layers.[2] The problem associated with the bulk graphite (002) reflection which obscures surface diffraction peaks with Q near 1.88 Å^{-1} does not exist in LEED. The orientation of the IC layer relative to the underlying graphite substrate can be easily obtained in LEED measurements. The combination of LEED data for the orientational epi-

taxy of the IC phases and neutron-diffraction data for modulation satellites has provided important information on the graphite-induced modulation of the IC phases of D_2 monolayers.[8]

In this paper we present LEED data and analysis for the IC H_2, HD, and D_2 monolayers on graphite. Our measurements show that the low-coverage α phase detected in the heat-capacity measurements[3-6] is a uniaxial IC (UIC) phase. The phase transition between the UIC phase and the higher-density rotated IC (RIC) phase appears very different for these three isotopes. For H_2 and HD monolayers the UIC phase and RIC phase are separated by a narrow region of fluid phase. For D_2 monolayers, a different kind of IC phase (the γ phase) was observed between the UIC and RIC phases. The LEED pattern of the γ phase is identical to that of a hexagonal heavy-domain-wall structure. The orientational epitaxy of both the γ and RIC phases was measured and compared with the continuum theory of Novaco and McTague. Various aspects of the γ phase are discussed. LEED data for the oriented fluid phases of H_2, HD, and D_2 are also presented and discussed.

II. REVIEW OF PROPERTIES OF ISOTOPIC HYDROGEN MOLECULES

H_2, HD, and D_2 are the simplest diatomic molecules in nature. The condensed phases of these molecules have prominent quantum effects which are due to the weak molecule-molecule interaction and the small molecular mass.[13] One of the quantum effects is the large translational zero-point motion (ZPM) of the single molecule. For instance, in the bulk H_2 solid the amplitude of the ZPM of a single molecule at $T=0$ K is as large as 18% of the lattice spacing. In contrast, the ZPM amplitude for bulk Kr is only 5%.[13] The ZPM will be even larger in

two dimensions[10] and thus will have a significant effect on the physisorbed monolayers. The existence of a C $(\sqrt{3}\times\sqrt{3})R\,30°$ phase for H$_2$ and its isotopes at submonolayer coverage[1,2] can be explained by the expansion caused by the ZPM, as in the case of He.[14] In fact, even for the heavier gas Kr model calculations show that the C $(\sqrt{3}\times\sqrt{3})R\,30°$ phase is not stable unless the zero-point energy is included.[15]

Another large quantum effect occurs because the rotational energy levels are well separated for H$_2$ and its isotopes. The energy difference between first excited rotational state $(J=1)$ and the ground state $(J=0)$ is 170 K for H$_2$ and 100 K for D$_2$.[13] Because the anisotropic molecule-molecule interaction is rather weak, the rotational state of the free molecule is preserved even in the solid phase at low densities.[13] Due to the symmetry requirement on the wave function two species of H$_2$ or D$_2$ molecules can be distinguished. *para*-H$_2$ and *ortho*-D$_2$ have an even rotational quantum number and a symmetric ground state $(J=0$ state); *ortho*-H$_2$ and *para*-D$_2$ have an odd rotational quantum number and an anisotropic ground state $(J=1)$. At low temperatures both *para*-H$_2$ and *ortho*-D$_2$ molecules equilibrate to the $J=0$ ground state and the interactions between the ground-state molecules are isotropic. The above selection rule does not apply to the heteronuclear molecule HD; at low temperatures, HD molecules are also in a $J=0$ isotropic rotational state. The adsorbate-substrate interaction affects the rotational states only slightly. This is confirmed by electron-energy-loss spectroscopy (EELS) measurements at $T<15$ K for H$_2$ physisorbed on Ag,[16] H$_2$, HD, and D$_2$ on Cu,[17] and H$_2$ on graphite.[18] By doing low-temperature experiments using *para*-H$_2$, *ortho*-D$_2$, and HD molecules, effects due to the pure isotropic molecule-molecule interactions can be separated from those of anisotropic molecule-molecule interactions.

III. EXPERIMENT

LEED measurements were performed at $5\le T\le12$ K. The experimental apparatus used in this experiment is the same as that of previous work on O$_2$ (Ref. 19) except for two modifications. A new thermal radiation shield which was originally designed for thermal-desorption measurements[20] was used in most of the measurements. Unlike the old radiation shield, which had a flat (0.6×1.0)-in.[2] rectangular window, the new radiation shield has a circular concave window with a 0.2-in. inner diameter. The new radiation shield significantly reduces the amount of thermal radiation received by the sample and sample holder. This enabled us to reach a temperature as low as 5 K, 2.5 K lower than that attained using the old radiation shield. The reduction in the thermal radiation is very important for observation of the H$_2$ UIC phase. Our first measurements using the old radiation shield did not detect the H$_2$ UIC phase at temperature around 8 K, which may be explained by the larger disturbance caused by the larger desorption effects. Indeed, H$_2$, HD, and D$_2$ monolayers condensed on cryosurfaces have a very large desorption rate induced by the room-temperature infrared radiation.[21] The electron beam was

also found to produce a large desorption of H$_2$, HD, and D$_2$ monolayers. The effect is largest for H$_2$ and considerably less for HD and D$_2$. One piece of evidence for electron-induced desorption is the observation of apparent (but false) coexistence of C and UIC, UIC and RIC, and sometimes C and RIC phases when the electron beam continuously bombards H$_2$ layers. This presumably occurs due to the nonuniform monolayer density distribution caused by electron-stimulated desorption which is proportional to the current density and thus is largest at the center of the beam and smaller away from the beam center. In order to reduce this effect the electron beam was turned on only for 0.5 s for photographing each LEED picture in most of our measurements. By doing so we are able to observe pure LEED patterns of UIC and RIC phases in the density ranges cited in this paper. These density ranges were not measurably altered when the time constant of the electron pulse was further reduced to 0.13 s. Therefore we feel that electron-stimulated desorption is no longer significant when a continuous electron beam is replaced by a 0.5-s electron pulse. The beam current was typically 0.3 nA in a beam with a full width at half maximum (FWHM) of about 0.5 mm.

Most of the data were collected from a Kish-graphite single crystal provided by H. Suematsu of the University of Tsukuba, Japan. The crystal was cleaved in air using cellophane tape and baked to 950 °C in dry flowing N$_2$ gas for about 10 min: 2 h were allowed for cooling down. Next, the crystal was clamped on a copper sample holder which was then installed in an ultrahigh-vacuum system. The background pressure in the vacuum chamber is about 2×10^{-10} Torr as indicated by a Bayert Alpert ion gauge. The temperature of the copper sample holder was measured by a silicon diode thermometer which was calibrated in the range 8–60 K. Temperatures below 8 K were estimated from the reading at liquid-He temperature and that at 8 K. The accuracy of the temperature measurement should be better than 1.0 K. The gases were admitted via a tube ending about 3 cm from the graphite sample to minimize the contamination due to impurity gases which are released when the H$_2$ gas pressure in the rest of the vacuum system rises. The gases used in our measurements were initially at room-temperature equilibrium ortho-para concentration ratios. The coverage of the monolayer was changed by varying the gas flux. A continuous flux of gas is required to attain a steady state for all of these isotopes. The difference in the infrared-induced desorption rate of these gases can be easily observed. At temperatures near 5 K, after the flux is stopped, the time required for the monolayer density to drop from 1.30 to 1.0 is observed to be 3 min for D$_2$ and less than 15 s for H$_2$.

The monolayer density of the IC phase was determined from the LEED pattern once the structure was deduced. The density ρ is normalized to 1 for the density of the C structure and is expected to agree with the real coverage if the amount of interstitials, vacancies, and second-layer adsorption is negligibly small. This assumption is well verified for IC D$_2$ by neutron measurements of the lattice constant of IC D$_2$ layers as a function of coverage.[8] Mea-

surements were made at several temperatures at various fluxes. A time interval of about 1–2 min was normally allowed between the change in flux and any measurement to ensure that steady-state conditions had been achieved. LEED pictures were taken using a 35 mm camera and Kodak Tri-X 400 ASA black and white film. The rotation angle and lattice constant of the IC phases were measured from projected images of the film. The accuracy of the measurements is estimated to be about 0.5° for rotation angle and 2% for density. The relative intensity contours of certain LEED reflections were measured from the film via a calibrated video camera interfaced to a Digital Equipment Corporation LSI 11/73 minicomputer.[22] The sharpest LEED features, observed in the RIC phase, had a FWHM of 0.05 Å^{-1}, which is an upper limit on the momentum resolution of the apparatus.

IV. RESULTS

The monolayer phases of H_2, HD, and D_2 are studied by varying the gas flux impinging on the graphite surface at a constant temperature. The stability of the temperature can be controlled to better than 0.2 K at 5 K, and 1.0 K at other temperatures. Figure 1 shows representative LEED photographs from the different phases. The bright area closest to the center is due to the overexposed (00) reflection. The C phase is shown in Fig. 1(a) for D_2. The UIC (α) phase is shown in Fig. 1(b) for H_2, Fig. 1(c) for D_2, and Fig. 1(d) for D_2 in coexistence with the γ phase. The γ and RIC phases for D_2 are shown in Figs. 1(e) and 1(g) and Fig. 1(f) shows the coexistence of the γ and RIC phases. Figures 1(h) and 1(i) show the oriented fluid phases of D_2 and HD. The structures and description of each of these phases will be presented in the following sections.

A. The UIC phase

The UIC phase, which corresponds to the α phase in the heat-capacity measurements, was observed for $1.07 < \rho < 1.14$ and $T = 5$ K for H_2 and D_2; for HD the upper density limit of the α phase at $T = 5$ K extends to
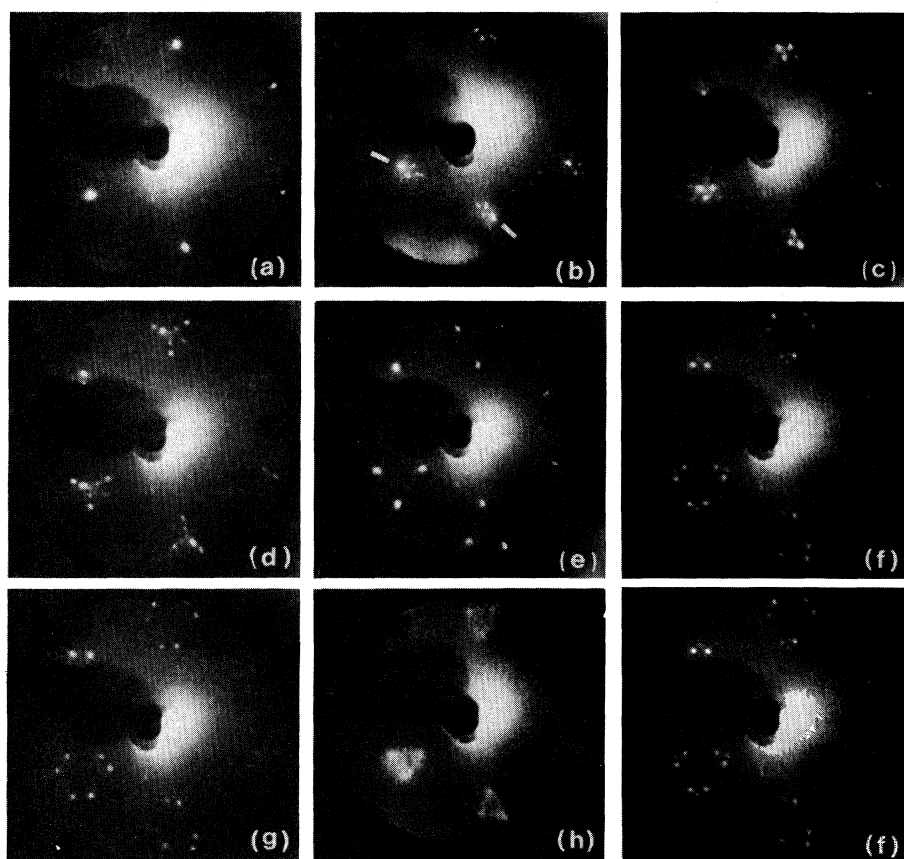

FIG. 1. LEED photographs taken at electron energy 62 eV. The electrons were incident slightly off normal from the Kish-graphite crystal; the angle in (b) is slightly different from the other figures. Due to asymmetric nucleation, the α spots in (b) and (d) are more intense for one of the three possible directions of compression [marked by lines in (b)]. (a) C phase of D_2 at 5 K. (b) α phase of H_2 at 5 K; $\rho = 1.13$. (c) α phase of D_2 at 5 K; $\rho = 1.12$. (d) Coexistence of the α and the γ phase of D_2 at 5 K; $\rho = 1.14$ for the α phase and 1.18 for the γ phase. (e) γ phase of D_2 at 5 K; $\rho = 1.27$. (f) Coexistence of the γ phase and RIC phase of D_2 at 5 K; $\rho = 1.31$ for the γ phase and 1.33 for the RIC phase. (g) RIC phase of D_2 at 5 K; $\rho = 1.36$. (h) β phase of D_2 at 10 K; $\rho = 1.15$. (i) β phase of HD at 10 K; $\rho = 1.18$.

1.18. LEED photographs of the UIC phase of H_2 and D_2 monolayers are shown in Figs. 1(b) and 1(c). One domain of a uniformly compressed UIC phase is shown in Fig. 2(a) and a representative section of the reciprocal space of the UIC phase is shown in Fig. 2(b). The peaks marked by the numbers 3, 4, and 7 in Fig. 2(b) correspond to the positions of a uniformly compressed UIC phase (i.e., positions of mean lattice diffraction) which are displaced relative to the C positions by ε, 2ε, and 3ε, where ε is equal to one-half of the lattice misfit. The rest of the peaks are possible satellites due to the lateral modulation induced by the graphite substrate. Such lateral modulation is described by modulation wave vectors which are given by the difference of the graphite and the nearest overlayer reciprocal-lattice vectors.[23,24] The arrow pointing from 7 to G represents one of the modulation wave vectors. Satellites are obtained by adding these vectors to the mean lattice positions. The diffraction pattern observed in LEED normally corresponds to the sum of three reciprocal-space pictures which are rotated 120° apart. Figure 2(c) shows $\frac{1}{3}$ of the diffraction pattern when only peaks 1–4 in Fig. 2(b) are considered. The observed LEED pattern [Figs. 1(b) and 1(c)] is consistent with this picture. As discussed in Appendix A, peaks 1 and 2 in LEED can also be produced by double-diffraction events involving sequential diffractions from a first-order graphite vector plus the overlayer reciprocal vectors corresponding to the mean lattice diffraction such as peaks 3 and 4 in Fig. 2(b). Therefore, information from LEED alone cannot simply determine the lateral modulation in the UIC phase. The quantitative description of the modulation in the UIC phase can be inferred from the neutron-scattering measurements.[5,7,8] Analysis of the neutron data indicates that the lateral modulation in the UIC phase can be described as a sharp striped superheavy-domain-wall network and the wall width is determined to be 2.8 (in units of the C-phase molecule row spacing of 3.66 Å) for H_2 (Ref. 5) and 2.5 for D_2.[8] (See Appendix A for more details.)

An asymmetric LEED pattern such as that shown in Fig. 1(b) was often observed at the beginning of an experiment on the Kish crystal. The LEED pattern in Fig. 1(b) is taken from the UIC phase of H_2. Such an asymmetric pattern has also been observed for the UIC phase of HD and D_2. [In Fig. 1(d) the D_2 pattern in coexistence with the γ phase has the same asymmetry as that for H_2 in Fig. 1(b).] The pattern shows that one of the UIC directions [marked by white lines in Fig. 1(b)] is nucleated much more than the other two on the crystal and provides clear evidence that the α phase is indeed a UIC phase. The mechanism which caused the asymmetric nucleation phenomenon is not well understood. We note that such an asymmetric LEED pattern was observed only when the gas was initially introduced onto the crystal. After cycling the coverage up and down a much more symmetric pattern, such as that shown in Fig. 1(c), appeared. We also note that the dominant nucleation direction was always the same. This leads to the tentative conclusion that the asymmetric nucleation is related to a greater number of steps along one direction of this particular Kish-graphite crystal. The adsorption is expected to be nucleated along the steps when these steps are clean and therefore the steps provide a preferential direction for further adsorption.

The UIC phase was also observed for the H_2 monolayer at $T=9$ K with the upper density limit reduced to 1.10. At temperatures near 10 K, only an oriented fluid phase such as that shown in Fig. 1(i) was observed between the C phase and the RIC phase. This observation is in good agreement with the maximum $T=9.7$ K for the α-β phase boundary[25] detected in H_2 heat-capacity measurements of Motteler[3] and of Freimuth and Wiechert.[4] For D_2 on graphite the UIC-phase pattern disappears at temperatures above 10 K. No measurements were made for D_2 at temperatures between 5 and 10 K. Nevertheless, the observation of a UIC phase at 5 K and a fluid phase at 10 K is also consistent with the maximum $T=7.2$ K for the α-β phase boundary from the heat-capacity measurements of Freimuth and Wiechert.[4,6]

Theoretically, for an isotropic adsorbate, the UIC phase is stabilized due to the energetics of the domain-wall crossings.[26–28] For an anisotropic adsorbate a weakly modulated UIC phase can also be formed because of the anisotropic elastic constants. For example, the UIC phase of N_2 on graphite[29] is believed to be due to the anisotropic interactions between N_2 molecules.[30] As
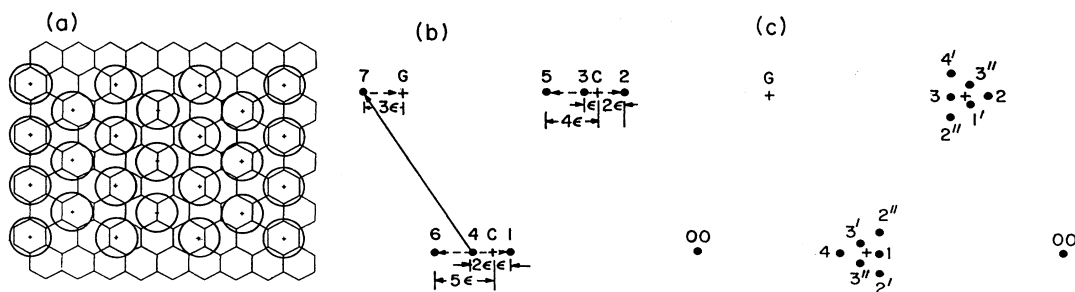

FIG. 2. The UIC phase. (a) Structure of a uniformly compressed UIC phase at $\rho=1.125$. The centers of the adsorbate molecules are indicated by crosses. (b) Reciprocal-space diagram of the structure shown in (a). Peak displacements from C positions are given in multiples of ε. The specular peak is denoted by (00); first-order commensurate peaks by C; first-order graphite peaks by G. Numbered peaks are discussed in text. (c) Diffraction pattern from three domains with peaks 1–4 of (b). The peaks denoted by primed and double-primed numbers are from the domains which are rotated by 120° and 240°, respectively, from that shown in (b).

mentioned previously, the gases used in the LEED measurements are normal H_2 and D_2.[31] Therefore the adsorbate could consist of both $J=0$ and $J=1$ molecules and the interaction between these molecules is not isotropic. On the cold graphite surface, the $J=1$ states would transform into the $J=0$ ground state due to local magnetic fields on the graphite surface. The transition rate was estimated to be 0.4% per hour for the C phase of H_2 on Grafoil and is about 6 times smaller for D_2 on Grafoil.[32] On the other hand, electron-energy-loss measurements suggest that the conversion of ortho-H_2 on pyrolytic graphite is almost instantaneous.[18] Therefore it is not clear how large the conversion rate is for the graphite single crystal used in the LEED measurements. Even so, the anisotropic molecules (molecules which are in a $J=1$ rotational state) are unlikely to provide the forces which cause the uniaxial compression due to following reasons: First, the orientational ordering temperature of $J=1$ molecules is less than 2.9 K for bulk H_2 and less than 3.9 K for bulk D_2.[13] For the C phase of ortho-H_2 on Grafoil the ordering temperature was detected to be 0.8 K; no orientational ordering was detected at $T>0.4$ K for the C phase of para-D_2.[32] Therefore, at $T \geq 5$ K, long-range orientational ordering of the $J=1$ molecules is not expected. Second, the high-temperature phase boundary of the UIC phase measured in LEED matches the same phase boundary of para-H_2 detected in heat-capacity measurements.[3,4] Third, the same UIC phase has also been observed for HD on graphite. Unlike H_2 and D_2, HD molecules equilibrate quickly into the $J=0$ ground state at low temperature, and the interactions between HD molecules are expected to be isotropic.

B. The C phase and C-UIC phase transition

The C phase of para-H_2 and ortho-D_2 on graphite was first identified in the neutron-scattering measurements.[1] The C phase of normal H_2 was also observed in the first LEED measurements.[2] A LEED photograph of the C phase of normal D_2 at an electron energy of 62 eV is shown in Fig. 1(a). The same C phase was also observed at several other electron energies in the range 40–140 eV. The intensity of the first-order LEED beams is maximized at 62 eV electron energy and is greatly reduced at energies above 70 eV. Similar intensity-energy dependence is also observed for the IC phase of D_2. For H_2 and HD only a smaller energy range (40–70 eV) was used. The intensity-energy dependence of both C and IC phases in this range is analogous to that of D_2. Due to the strong forward scattering of the H_2, D_2, and HD molecules,[33] the primary scattering is expected to be sequential overlayer-substrate double scattering and thus the intensity of the graphite specular and first-order beams will strongly affect the observed overlayer intensities. Data from other studies[34] indicate that both specular and first-order graphite beams are maximum near the 62 eV electron energy used for the measurements presented here.

The C-UIC phase transition was examined in detail by LEED for H_2; two-dimensional (2D) intensity contour maps are shown in Fig. 3. A charge-coupled-device (CCD) video camera was used to digitize LEED photos[22]
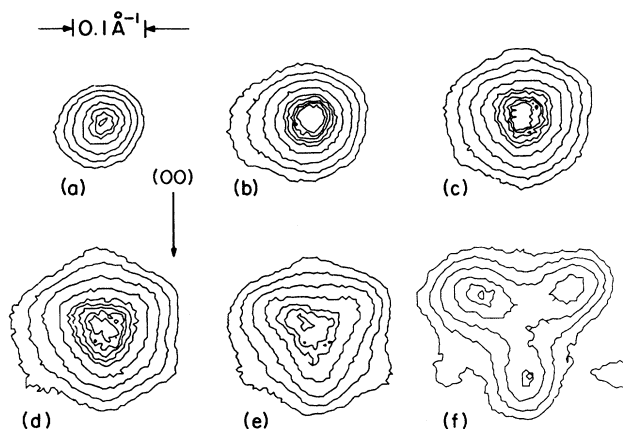

FIG. 3. Two-dimensional intensity contours of a H_2 LEED first-order beam at $T=5$ K when ρ increases from a value near 1.0 to 1.09. The lowest relative intensity level is 0.1; the increment is 0.1 along an inward direction pointing to the diffraction maximum. The arrow indicates the direction of the (00) reflection. The relative pressures at a quadrupole mass spectrometer are (a) 1.50, (b) 2.00, (c) 2.10, (d) 2.15, (e) 2.30, and (f) 2.60.

including several calibration photos taken at different electron-beam currents; the contour maps of the scattering intensity were produced on a VAX 11/780 computer using plotting routines developed by the Astronomy Department of the University of Washington. Under the experimental conditions used the local pressure of the gas near the sample could not be directly measured; instead the relative background gas pressure in the vacuum chamber was measured by a quadrupole mass spectrometer. This pressure is a monotonically increasing function of the local pressure of the gas impinging on the sample. Figures 3(a) and 3(b) are taken at relative pressures $P=1.50$ and 2.00. The change in intensity from Fig. 3(a) to 3(b) is due to completion of the C layer. As indicated by Figs. 3(c)–3(e), at higher pressures ($P=2.10$, 2.15, and 2.30) the LEED peak becomes wider and the intensity maximum starts to drop. At the largest pressure shown ($P=2.60$), the three strong reflections and one or two of the weak reflections can be seen in Fig. 3(f) and the density of the UIC phase reaches 1.09 measured from the amount of splitting of LEED spots. The resolution of the data in Fig. 3 is sufficient to rule out a first-order C-UIC transition with density jump greater than 5%. Theoretical predictions[26,27] allow a continuous C-UIC phase transition, but due to the uncertainty in determination of the structure at densities below 1.05 we cannot say whether the observed phase transition is continuous. The precision of the data was judged to be insufficient to justify a quantitative comparison with possible C-UIC phase coexistence. In addition, there could be some small residual false coexistence produced by electron-induced desorption in this density range for H_2 (see Sec. III).

C. The RIC and γ phases

At $T=5$ K a phase transition from the UIC phase to higher-density IC phases occurs when the gas flux is in-

creased beyond the value which produces the most compressed UIC phase. For H_2 and HD monolayers this transition is from a UIC phase to a RIC solid phase [such as Fig. 1(g)] via a narrow fluid phase [as in Fig. 1(i)]. The symmetry of the fluid phase inferred from the LEED pattern is analogous to that of the RIC phase and will be discussed in more detail in Sec. IV E. The RIC phase has a triangular unit mesh and a rotation away from the C-phase orientation by $\theta = 4°-8°$ in the density range 1.24–1.56. For the D_2 monolayer an additional incommensurate solid phase [γ, Fig. 1(e)] was also observed between the UIC phase and the RIC phase. The observed coexistence of γ-UIC [Fig. 1(d)] and γ-RIC [Fig. 1(f)] indicates first-order phase transitions. The structure of the γ phase inferred from the LEED pattern is the same as the RIC phase, except for the lattice orientation θ relative to the C phase. Figure 4(a) shows structure of a uniformly compressed and rotated γ phase of D_2 at $\rho = 1.25$ and $\theta = 9.0°$. Figures 4(b) and 4(c) show $\frac{1}{6}$ of the diffraction pattern from one domain of the γ and the RIC phases. Peaks 4 and 8 in Figs. 4(b) and 4(c) correspond to first- and second-order diffraction of one rotational domain of the uniformly compressed lattice. Peaks 1–3 and 5–7 are possible satellites due to the modulation of the nearest-neighbor distances of the adsorbate molecules by the periodic substrate field. The positions of these satellites are obtained by adding the modulation wave vectors (such as that indicated by the arrow pointing from 8 to the graphite peak G) to the mean lattice peaks (such as peak 4).[23,24] The observed LEED pattern is consistent with peaks 1, 3, and 4 in Figs. 4(b) and 4(c). These peaks can be explained by the first-order mean lattice diffraction peaks [peak 4 in Figs. 4(b) and 4(c)] plus the peaks due to the sequential scattering (double scattering) from first-order graphite vectors and first-order reciprocal vectors of the overlayer. The geometry of the double scattering from the RIC phase is the same as that from the RIC phase of Ar.[35] The geometry of the double scattering from the γ phase reduces the number of observed peaks by half, as explained in Appendix B. In the LEED measurements performed so far satellite peaks 2 and 5–7 were not observed in either the RIC or the γ phases (satellite peaks 1 and 3 always coincide with

double-scattering spots). In contrast, the satellites marked by 2 and 5 for the γ phase were observed in the neutron-diffraction measurements[6,8] in addition to the main reflection due to the peak 4; no satellites were observed for the RIC phase.

The orientation angles of the γ phase of D_2 and the RIC phases of H_2, HD, and D_2 are presented in Fig. 5. Curve (b) in Fig. 5 is the result of Novaco and McTague's (NM) (Ref. 23) theoretical model for the two-dimensional Cauchy solid. All the data for the RIC phase are consistent with NM's result except for some small deviations; however, the γ phase has a rotational epitaxy completely different than the theoretical NM prediction. The disagreement between the rotational epitaxy of the γ phase and the prediction of NM's linear theory also shows up when comparing the direction of the modulation wave vector (the difference of the graphite reciprocal-lattice vector and the nearest overlayer reciprocal-lattice vector) for the two phases. For the γ phase the direction of this vector, as indicated in Fig. 4(b), is always along a high-symmetry direction of the graphite, leading to curve (a) in Fig. 5, given by $\sqrt{\rho} = \sin 60°/\sin(60° - \theta)$. However, in NM's linear theory, this vector is predicted to be along a nonsymmetry direction of the substrate,[23] as in Fig. 4(c).

Another interesting aspect of the γ phase is that it has a diffraction pattern identical to a hexagonal heavy-domain-wall phase[24,36] which suggests the two structures must be topologically similar. The relation of the structure of the γ phase with a hexagonal heavy-domain-wall phase and a kinematic diffraction-intensity calculation based on a higher-order 4×4 commensurate structure are presented in Appendix B.

D. Discussion of the rotational epitaxy of the γ phase of D_2

As mentioned previously, the γ phase has a special rotational epitaxy which has not yet been predicted by any theoretical calculation. The agreement between the satellite positions measured by neutron diffraction and the orientations measured by LEED,[8] on the other hand, suggests that a strong substrate-induced modulation is responsible for the orientation of the γ phase. Substrate-induced modulation is the same mechanism proposed by
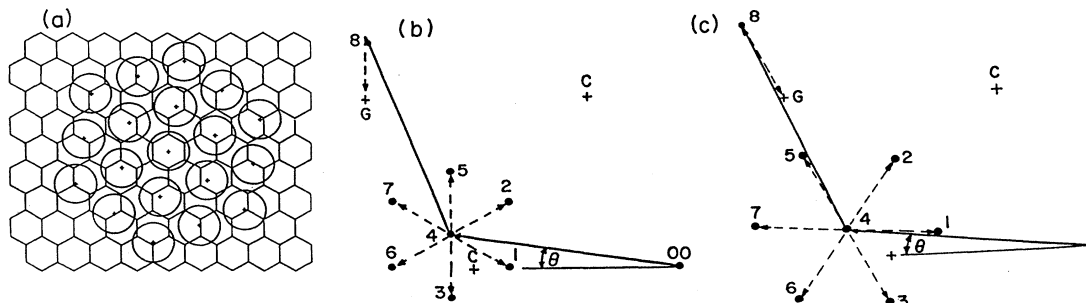
FIG. 4. The γ and RIC phases. (a) Structure of the uniformly compressed and rotated γ phase at $\rho = 1.25$ and $\theta = 9.0°$. The structure of the RIC phase is analogous to that in (a) with rotation angle $3°-5°$ smaller than that of the γ phase. (b) and (c) The reciprocal-space diagrams of the γ and RIC phases at $(\rho, \theta) = (1.25, 9°)$ and $(1.42, 7°)$, respectively. C-phase positions are indicated by crosses. The numbered peaks are discussed in the main text.
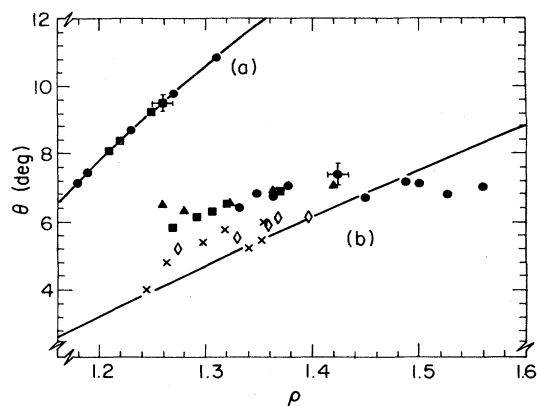
FIG. 5. Rotation angle (θ) vs monolayer density (ρ) determined from LEED measurements for the D_2 γ phase and RIC phases of D_2, H_2, and HD at $5 < T < 12$ K. The upper curve, (a), is determined by the requirement that the modulation wave vector of the γ phase is along the graphite symmetry direction as in Fig. 4(b); the lower curve, (b), is the NM result (Ref. 21) with the central-force sound-velocity ratio. The solid circles, squares, and triangles are D_2 data taken at 5, 10, and 12 K, respectively. HD and H_2 data at 5 K are indicated by crosses and diamonds. Error bars show typical measurement uncertainties.

Novaco and McTague[23] for the rotation of an IC triangular phase physisorbed on the graphite substrate. Their calculation, however, is only appropriate for a weakly modulated IC phase because it assumes an IC triangular lattice which interacts so weakly with the underlying substrate that only the linear term of the substrate field needs to be taken into account. The orientations for IC phases of Ar (Ref. 35) and Ne (Ref. 37) on graphite were calculated[23] using the microscopic interaction parameters of these molecules and are in good agreement with experimental data. No neutron-scattering modulation satellites were observed for these rotated incommensurate layers,[38,39] indicating that they are indeed weakly modulated structures. The observation of satellites in the γ phase by neutron diffraction[6,8] suggests that the modulation in the γ phase is bigger than that in the RIC phases of H_2, HD, D_2, Ar, and Ne, and, therefore, NM's linear theory may not be appropriate for such an IC phase.

The NM model can, in principle, be extended to include the nonlinear effects of the substrate field. Preliminary calculations using the method of self-consistent phonons and the lowest-order nonlinear term of the substrate corrugation potential for H_2 and D_2 on graphite procedures a good agreement with our data only for the RIC phase.[40] This fact suggests that a more accurate calculation of the substrate lateral modulation should be performed. Shiba has performed the most complete continuum model calculation for Kr on graphite.[41] The model has one adjustable parameter which allows application to systems other than Kr. In this calculation the periodic substrate-adsorbate potential was approximated by its first-order Fourier series, which is more accurate than its linear expansion. The result showed a continuous transition from a nonrotated IC structure to a rotated IC structure. The rotation angle was found to be smaller than

that predicted by NM's linear theory at the regime near the nonrotated-to-rotated (NR-R) transition and to approach it at the regime away from the NR-R transition for a range of the parameters. Experimental results for Kr are in a good agreement with this model calculation.[11,42] In the case of H_2 and its isotopes the continuum approximation used in Shiba's calculation may not be valid because the large ZPM for H_2 and its isotopes expands the lattice far beyond the classical minimum in the pair potential, which results in a very soft response to the external strain. For example, the molar volume of three-dimensional (3D) solid H_2 decreases by a factor of 2 when the pressure increases from zero to 10 kbar.[13] As a comparison, the molar volume of the ordinary 3D solid in which the molecules interact via van der Waals forces usually changes by only a few precent for the same pressure change.

We believe the existence of the γ phase is related to the fact that the ratio of effective adsorbate-adsorbate coupling to the adsorbate-substrate coupling in a D_2 monolayer is smaller than that in H_2 and HD monolayers due to the relatively smaller ZPM of the D_2 molecules. The relatively weaker coupling ratio for a D_2 monolayer is suggested by the calculated phonon spectrum for C-phase H_2 and D_2 on graphite at $T=0$ K.[40] The difference between the maximum and minimum phonon energy is 15 K for C-phase D_2 and 40 K for C-phase H_2. The spread in the phonon spectrum of commensurate H_2 is primarily due to the increased effective adsorbate-adsorbate interaction. A weaker adsorbate-adsorbate interaction compared with the adsorbate-substrate interaction leads to a flatter phonon spectrum. For a physisorbed IC monolayer the weaker adsorbate-adsorbate interaction means that the effects of the lateral adsorbate-substrate modulation are larger. This causes the adsorbate to be oriented along a direction different from that predicted by a theory which assumes weak substrate modulation. The effective adsorbate-adsorbate interaction can be increased by either increasing the temperature or increasing the monolayer density. In both cases, a phase transition from the γ phase to the RIC phase was observed.[6]

E. Fluid phases

The β phase of H_2 and D_2 observed in the heat-capacity measurements[3-5] was determined to be an oriented fluid phase. The LEED patterns of the β phase are shown in Figs. 1(h) and 1(i). The LEED spot has a much larger radial width (FWHM of 0.1–0.2 Å^{-1}) than for the solid phase (FHWM of 0.05 Å^{-1}), indicating a short-range translational correlation. The LEED spot also has a finite azimuthal width, indicating that the β phase is well oriented relative to the graphite substrate. The local structure inferred for the β phase of both H_2 and D_2 has a triangular nearest-neighbor arrangement. The orientation relative to the substrate is very different when D_2 is compared to H_2 and HD. The β phase of H_2 is oriented along the C-phase direction, and the radial and azimuthal width (FWHM) of a LEED spot at density 1.18 are 0.10 and 0.15 Å^{-1}, respectively. As shown in Fig. 1(h), the orientational epitaxy of the β phase of D_2 is

the same as the γ phase, which suggests that the β fluid of D_2 is due to the disordering of the γ phase. Fluid phases oriented along the C $(\sqrt{3}\times\sqrt{3})R\,30°$ phase direction were also observed previously for Ar,[43] O_2,[44] Xe,[45] and C_2H_6 (Ref. 46) on graphite.

One possible orientational ordering in the two-dimensional fluid phase is associated with the melting of a two-dimensional (2D) solid. It was first proposed and discussed by Kosterlitz and Thouless (KT) that the melting transition in a 2D system is mediated by topological defects.[47] The model was later extended to the physisorbed-monolayer case by Nelson, Halperin, and Young (KTHNY).[48,49] They predicted that the melting of a 2D solid on a smooth substrate can proceed in two stages. In the first stage the layer loses its quasi-long-range translational ordering but still has a quasi-long-range bond-bond orientational ordering and forms a hexatic fluid phase; at the second stage the layer loses both translational and bond-bond orientational ordering and becomes a true fluid. The effect of periodic substrate field has also been considered.[48] It turns out that the fluid phase can always have quasi-long-range bond-bond correlation due to a sixfold substrate field. The effect discussed by KTHNY will only affect the ratio of the radial and azimuthal width.[45] Therefore the information on bond orientational order of the fluid phase alone cannot determine the origin of such ordering.[45] However, the observation of different orientations of the H_2 and D_2 fluid suggests a strong influence of the substrate field. The analogous LEED patterns of the γ and β phases of the D_2 monolayer also suggest that the orientation of the fluid phase might be due to the same effect of the substrate field which causes the rotation of the γ solid phase.

V. SUMMARY

Our LEED measurements for H_2, HD, and D_2 on graphite have detected several IC phases which were not identified in the earliest neutron-scattering and LEED measurements.[1,2] The α phase detected in the heat-capacity measurements was determined to be a UIC phase. The existence of such a UIC phase qualitatively agrees with the corresponding theoretical work.[27,28] The γ phase, which has a different rotational epitaxy from the high-density RIC phase, was detected for D_2 on graphite. The rotational epitaxy of the RIC phase was measured; in this case our data qualitatively agree with the continuum theory of Novaco and McTague.[23]

Figure 6 shows the phase diagram we have constructed by combining our LEED data with data from heat-capacity[4,6] and neutron-diffraction[7,8] measurements for D_2 on graphite. In the heat-capacity measurements[6] the monolayer coverage was normalized to the coverage which produces the largest C-phase disordering signal. That coverage was found to be 3.3% higher than the density ρ deduced from the lattice constant measured by neutron diffraction.[6] Therefore, in constructing Fig. 6 all the heat-capacity data are corrected by a factor of 3.3% in coverage.[25] The solid lines in Fig. 6 indicate the phase boundaries inferred from the experimental data and dashed lines indicate phase boundaries which are less cer-

tain. There is no conclusive information available for the overlayer at ρ between 1.0 and 1.05. The α phase occurs at ρ near 1.10. The disordering of the α phase occurs, according to the heat-capacity measurements,[5] at $T=7.2$ K in the range for coverage from 1.07 to 1.15. The heat-capacity data also suggest that a triple line exists between the α and β phases. The α-γ transition is first order, as indicated by Fig. 1(d). This information leads to the phase boundaries as shown in Fig. 6 at $1.07<\rho<1.15$ and $6.5<T<8.5$ K. Analogous features in the heat-capacity data also suggest another triple line located at T near 11 K and ρ near 1.25. Therefore, phase boundaries near the second triple line should be analogous to those near the first one. In neutron and LEED experiments made so far, the δ and ε phases identified in heat-capacity measurements are indistinguishable from the γ phase. We believe that the δ and ε phases are most likely higher-order commensurate phases with the same rotation angle versus density as the γ phase. The possible higher-order C
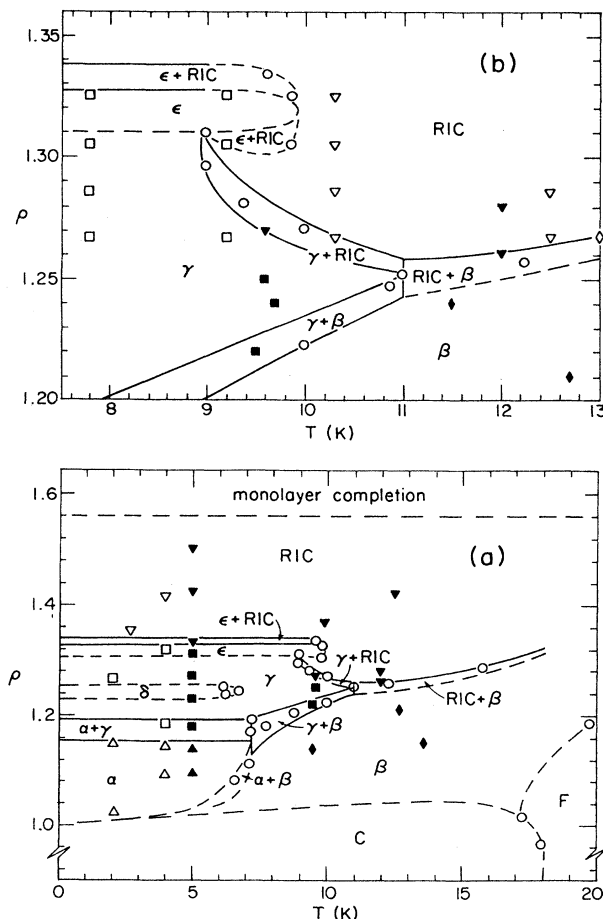

FIG. 6. Proposed phase diagram for the D_2 monolayer on graphite. Heat-capacity peaks are indicated by open circles. Solid triangles (α phase), squares (γ phase), diamonds (β phase), and inverted triangles (RIC phase) are data measured by LEED. Open triangles, squares, and inverted triangles are a few of the many data points measured by neutron diffraction (Ref. 6). (a) $1.0<\rho<1.6$, $T<20$ K. (b) $1.20<\rho<1.35$, $7.5<T<13$ K.

phases are $(4 \times 4)(\rho = 1.31)$ and $(5\sqrt{3} \times 5\sqrt{3})R\,30°(\rho = 1.24)$ structures.

APPENDIX A: DOMAIN-WALL STRUCTURE IN THE UIC PHASE

The modulation in the a UIC phase of H_2, HD, and D_2 monolayers on graphite is described by a network of striped–superheavy domain walls.[5-8] In this appendix the diffraction intensity from such a domain-wall structure is calculated and compared with LEED measurements. Effects of thermal fluctuations of the domain walls and effects of multiple scattering in LEED are also discussed.

In the striped–superheavy–domain-wall phase the commensurate domains are separated by parallel dense domain walls. Figure 7(a) shows an example of striped–superheavy–domain-wall phase in the lattice-gas limit at $\rho = 1.125$. The separation between the domain walls is $5.33b$ for the structure shown in Fig. 7(a) and is $D = (N - \frac{2}{3})b$ for a general case,[24] where N is the number of molecule rows in each commensurate domain, b is the row spacing of the C-phase lattice $[b = (\sqrt{3}/2) \times 4.26 = 3.69$ Å$]$, and $a = 4.26$ Å is the period in the unmodulated direction. The structure in Fig. 7(a) can also be described by a superlattice structure with the unit cell indicated by dashed lines.[24] The reciprocal lattice can be constructed from D and a and is shown in Fig. 7(b). The primitive vectors of the reciprocal lattice are shown by τ_1 and τ_2 with $\tau_1 = Q_c / (N - \frac{2}{3})$ and $\tau_2 = (\sqrt{3}/2)Q_c$, where $Q_c = 1.703$ Å^{-1} is the length of the reciprocal-lattice vector of the commensurate phase. Diffraction patterns can be obtained by adding three reciprocal-space pictures which are oriented 120° apart. If only the peaks which are nearest (peaks marked 1 and 3) and next nearest (peaks marked 2 and 4) to the C-phase (cross) primary peak are considered, the diffraction pattern from such a striped phase would be exactly the same as that shown in Fig. 2(c).

The scattering amplitude from such a periodic structure[24] can be calculated by

$$S(\mathbf{Q}) = \sum_i f_c(\mathbf{Q})\exp(i\mathbf{Q}\cdot\mathbf{R}_i) \ , \qquad \text{(A1)}$$

where $f_c(\mathbf{Q}) = \sum_j \exp(i\mathbf{Q}\cdot\mathbf{r}_j)$ is the structure factor, $\mathbf{r}_j$ measures the distance of each molecule relative to some reference position in the unit cell, and $\mathbf{R}_i = m_1\mathbf{D} + m_2\mathbf{a}$ measures the distance of the unit cell from the origin (m_1
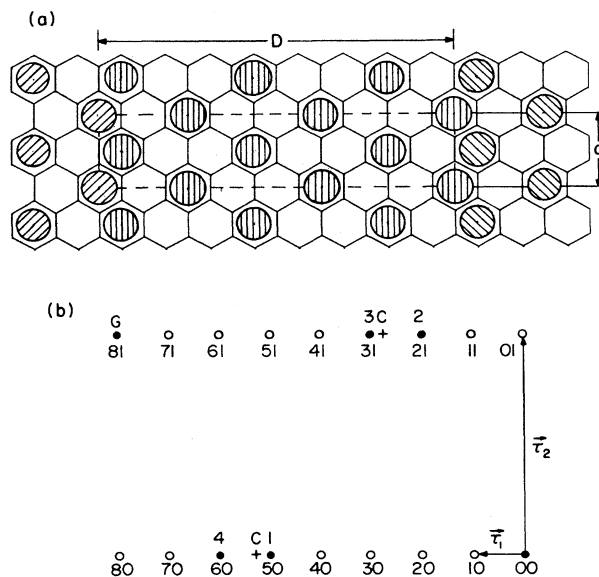

FIG. 7. The striped–superheavy-domain-wall UIC phase at $\rho = 1.125$. (a) Real-space structure. A unit cell of size D by a is indicated by dashed lines. Different shadings indicate the three sublattices of the lattice-gas limit. (b) Reciprocal lattice corresponding to the structure in (a). τ_1 and τ_2 are reciprocal-lattice primitive vectors. Solid circles indicate the peaks observed in LEED; numbers above these circles correspond to the same peaks in Figs. 2(b) and 2(c).

and m_2 are integers). In writing (A1) we assume that each molecule is a point scatterer and neglect the effects of thermal fluctuations and multiple scattering. A pure two-dimensional structure is also assumed since both neutron scattering and LEED forward scattering are most sensitive to in-plane displacements.[50] Diffraction peaks occur when $\mathbf{Q}$, which is proportional to the in-plane momentum transfer of the scattering particles (electron, neutron, etc.), is equal to a reciprocal-lattice vector of $\mathbf{R}_i$. The relative intensities of these diffraction peaks can be calculated from the structure factor if the relative positions of each molecule inside the unit cell, which can be determined from a given domain-wall profile, are given. The domain-wall profile used in this calculation is that derived by Gordon and Lançon[51] and is given by

$$X_l = (l - \tfrac{1}{6})b - (4b/3\pi)\tan^{-1}\{\exp[(l - 0.5)\pi/w]\} \ , \qquad \text{(A2)}$$

where X_l is the abscissa of the lth molecular row relative to the domain-wall center, and w is the domain-wall width given in the units of molecular row spacing in the C phase. Only the nearest domain wall is considered in determining the positions of each adsorbate molecule. The calculated intensities for the structure shown in Fig. 7(a) are presented in Table I. Intensities measured by LEED are also shown. In LEED measurements the peaks which correspond to (5,0), (6,0), (2,1), and (3,1) in Fig. 7(b) or 1, 4, 2, and 3 in the general case shown in Fig. 2(b) were observed. The calculated intensities of these

peaks as a function of density ρ for domain-wall widths $w=0.0$ and 2.8 are shown in Fig. 8. For the uniformly compressed UIC phase one would only observe peaks 3 and 4. The observation of satellite peak 1 in neutron-scattering measurements[5-8] provides clear evidence that the structure of the UIC phase is modulated by the adsorbate-graphite interaction. The wall width can be inferred by fitting the data from the neutron-diffraction measurements to the calculation. By comparing the relative intensities of the neutron-scattering peaks 1–3 with analogous calculations, the wall width was determined to be 2.8 for H_2 (Ref. 5) and is 2.5 for D_2.[8]

Table I shows that the intensities measured by LEED do not fit the calculated intensities for $w=2.8$. This is primarily due to the effects of multiple scattering: The dominant effect of multiple scattering is due to the sequential scattering (double scattering) from the graphite and the overlayer. (As mentioned in the text, forward scattering is much larger than backscattering for molecular hydrogen.[33]) In LEED there are two types of dominant double-scattering events. The first one is due to a sequential scattering of a graphite (00) backreflection and a forward scattering from the overlayer or vice versa. This kind of double-scattering event has an intensity which is affected by the graphite (00) reflection; it does not produce new diffraction beams, but it does affect the scattering intensity. The other kind of relevant double-scattering events are due to the sequential scattering from a first-order graphite backreflection and a forward scattering from the overlayer or vice versa. This process can in general produce diffraction beams[35] which are not degenerate with those of "single scattering." Figure 9 shows some of the double-scattering events produced by adding vectors corresponding to the (6,0), (2,1), (3,1), and (5,0) beams to the vectors corresponding to first-order graphite beams. Other double-scattering events can be

obtained by reflecting Fig. 9 with respect to the horizontal and vertical axes. No new diffraction beams are generated in this case. As indicated in Fig. 9, the double-scattering process produces diffraction beams which are distinct from the beams from domains rotated 120° apart. Because of this it is possible to observe nonuniform nucleation of the UIC phase in LEED. It is also obvious that each beam observed in the UIC phase by LEED is actually the sum of the diffraction beams due to the single scattering and those due to the double scattering. For example, the intensity of the (5,0) beam is due to the single-scattering event (5,0) and two double-scattering events which correspond to sequential diffraction from graphite [(8,1) or (8,−1)] and from the [(−3,1) or (−3,−1)]. Therefore in LEED the intensity of the (5,0) beam depends on intensities of both the (5,0) and (3,1) beams, as well as of the graphite (00) and (10) beams. This is the main reason for the deviation of LEED intensities from those given by a kinematic calculation.

Another discrepancy between the calculation and experimental observations is that at $w=2.8$ the (7,0) peak is predicted to be more intense than the (5,0) peak that was observed in neutron-scattering measurements. Neither LEED nor neutron scattering observed the (7,0) peak. The (7,0) peak is significantly altered by thermal fluctuations of domain walls which cause the intensity of this peak to be much lower than that of static calculations. In the sharp wall limit, the major effect of thermal fluctuations of domain walls is to cause the intensity of each diffraction peak to decay as a power law,[52-54]

$$I(\mathbf{Q}) \sim (\mathbf{Q} - \boldsymbol{\tau})^{-2+\eta}, \tag{A3}$$

where τ is the overlayer-lattice vector. If we designate the peaks nearest to commensurate positions as first harmonic, then the other peaks can be designated as second or higher harmonics depending on the separation be-

TABLE I. Calculated intensities from the structure presented in Fig. 7. $I(w=0.0)$, $I(w=2.8)$, and $I(w=\infty)$ stand for the intensities calculated for wall width w [defined by Eq. (A2)] equal to 0.0, 2.5, and ∞, respectively. I_{LEED} is the intensity measured for H_2 by LEED at $\rho=1.10$ and an electron energy of 62 eV. The calculated intensities are normalized to the intensity of the (0,0) beam, and I_{LEED} is normalized to the intensity of (3,1) beam. The asterisk indicates intensity which is not measurable due to the degeneracy with the graphite reflection.

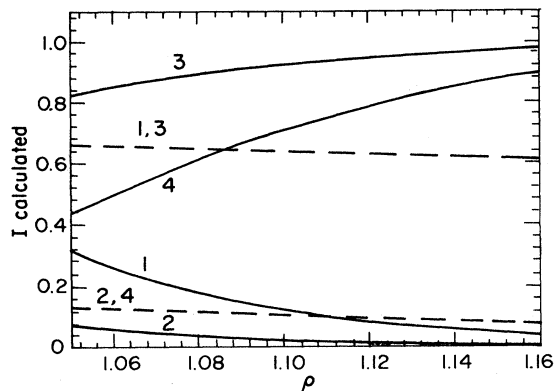| m	n	$I(w=0.0)$	$I(w=2.8)$	$I(w=\infty)$	I_{LEED}
0	0	1.00	1.00	1.00	*
1	0	0.01	0.00	0.00	0.00
2	0	0.02	0.00	0.00	0.00
3	0	0.03	0.00	0.00	0.00
4	0	0.06	0.00	0.00	0.00
5	0	0.62	0.10	0.00	0.85
6	0	0.10	0.72	1.00	0.15
7	0	0.01	0.16	0.00	0.00
0	1	0.00	0.00	0.00	0.00
1	1	0.01	0.00	0.00	0.00
2	1	0.10	0.02	0.00	0.23
3	1	0.62	0.93	1.00	1.00
4	1	0.06	0.06	0.00	0.00
5	1	0.03	0.00	0.00	0.00
6	1	0.02	0.00	0.00	0.00
7	1	0.01	0.00	0.00	0.00

FIG. 8. Calculated intensities of peaks 1–4 in Fig. 2(b) in the density range $1.06 < \rho < 1.15$. Dashed lines are calculations for the wall width $w=0.0$ and the solid lines are for $w=2.8$.

tween the peak considered and the nearest commensurate position. As discussed by several authors, the decay exponent obeys $\eta = 2s^2/p^2$, where s is the order of harmonic and $p=3$ for this system.[52,53] This result indicates that a higher harmonic has a larger part of its intensity at the tails than that of a lower one. Equation (A3) also indicates that, for a given system, only a finite number of harmonics can be observed. The highest observable harmonic can be determined by $\eta(s)=2$. This implies that third harmonics would vanish for the striped phase of H_2 on graphite if the walls are very narrow as in Fig. 7(a). For a system where the walls have finite width, the effect of domain-wall fluctuations may not be as large as the case
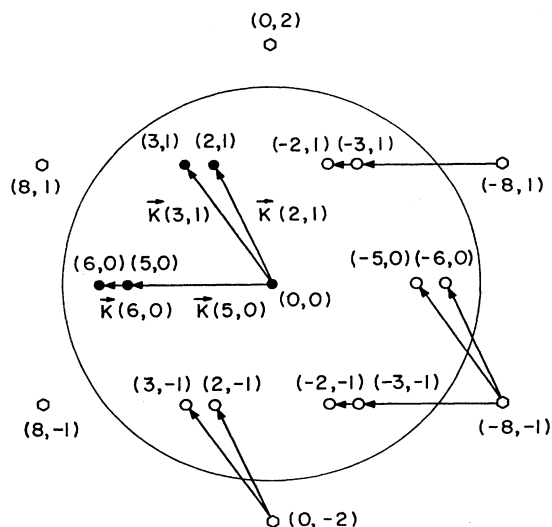

FIG. 9. Schematic diagram of some double-scattering events due to the sequential scattering from the UIC phase shown in Fig. 7 and graphite. The solid circles are the positions of some of the direct scattering given by the kinematic calculation; open circles indicate scattering events which are obtained by adding the vectors corresponding to direct scattering to the graphite beams (hexagons); the large circle indicates the typical range observed in our LEED apparatus at electron energy near 60 eV.

of very narrow (sharp) walls. However, it is possible that thermal effects are still big enough to cause some of the higher-order harmonics to disappear or be too small to be observed experimentally. This may be the reason that the (7,0) peak was not observed. It should be pointed out that a similar phenomenon was also observed for the weakly incommensurate Kr monolayer on graphite which has a hexagonal superheavy-domain-wall structure.[11,36] In the Kr case a predicted satellite which is a second harmonic according to the designation described above was not observed in the synchrotron x-ray measurements. It is very likely that the unexpected low intensity of the satellites is due to the same mechanism in both cases.

In Ref. 7, a static domain-wall structure with a variation in wall separations at each density was used to fit the neutron intensities from D_2 on ZYX graphite. It seems likely that the equilibrium fluctuations of the domain walls are the actual physical mechanism causing the observed intensity distribution. For example, the domain-wall fluctuations will cause peaks 2 and 4 to appear to have less intensity than predicted by a periodic and static domain-wall structure, resulting in the type of relative intensity distribution observed in Ref. 7.

APPENDIX B: THE γ-PHASE STRUCTURE

The γ phase of the D_2 monolayer physisorbed on the graphite substrate has been determined to be a modulated and rotated IC phase.[8] One interesting aspect of the γ phase is that the orientation (relative to the substrate) of this phase is always along a special direction such that it produces a LEED pattern which is identical to that from a hexagonal heavy-domain-wall structure. This interesting fact suggests that the topological structure of the γ phase should be analogous to that of a hexagonal heavy-domain-wall phase.

A hexagonal heavy-domain-wall phase is a domain-wall phase in which the commensurate domains are separated by a hexagonal heavy-domain-wall network.[24,55] Examples of such a domain-wall phase are shown in Figs. 10(a) and 10(d). The corresponding reciprocal lattices are shown in Figs. 10(c) and 10(f). The peaks marked by 1, 3, and 4 are nearest to the C-phase position (cross), and in the lattice-gas limit, are strongest in intensity. The rest of the peaks are higher-order peaks and much weaker than peaks marked by 1, 3, and 4. Comparing positions of peaks 1, 3, and 4 in Figs. 10(c), and 10(f) with those in Fig. 4(b), one can easily find out that they are actually identical if the density of the latter structure is equal to 1.31 or 1.16, respectively.

The relation between the γ phase and a hexagonal heavy-wall phase can also be shown in the real-space picture. Figure 10(b) shows a picture of an unmodulated uniform-spacing γ phase at density 1.31. At this density, the γ phase matches a (4×4) commensurate structure. The short arrows in Fig. 10(b) indicate the direction of the forces which are caused by adsorbate-substrate interactions. Comparing this structure with the hexagonal heavy-domain-wall structure presented in Fig. 10(a), one finds that these two structures are topologically identical. This means that one can get the hexagonal heavy-
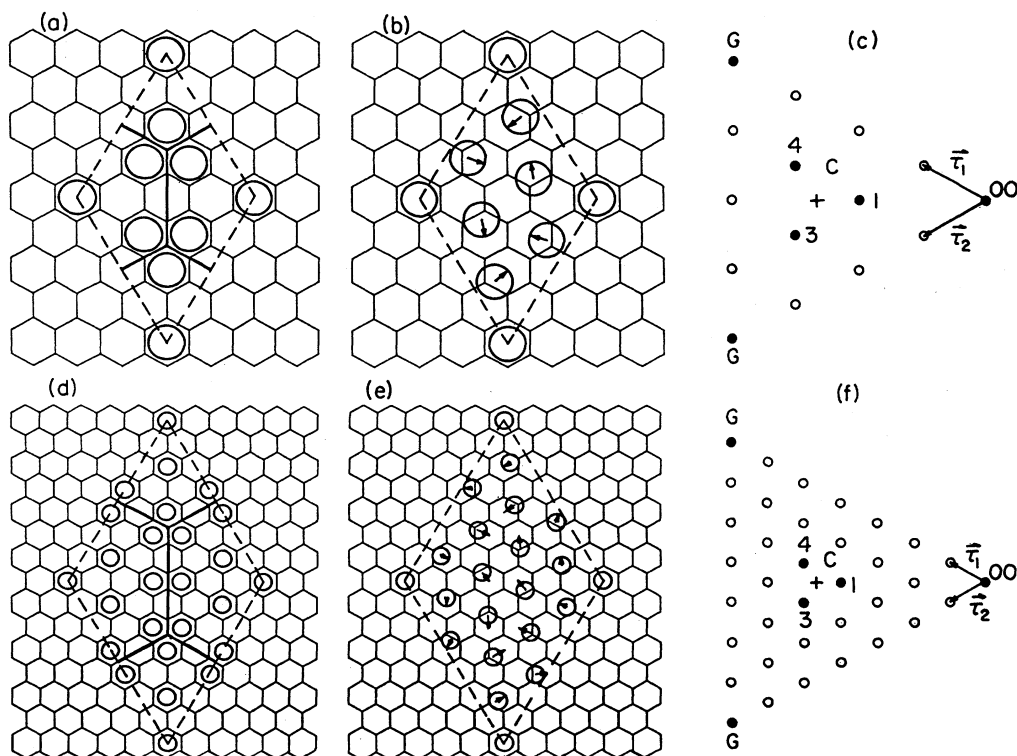
FIG. 10. Possible γ-phase structures. (a) and (d) show a hexagonal heavy-domain-wall phase at densities of 1.31 and 1.16. The unit cell is indicated by dashed lines and domain walls are indicated by solid lines. (b) and (e) show (4×4) and (7×7) higher-order commensurate uniformly compressed triangular structures which have the same orientation as that of the γ phase at $\rho=1.31$ and 1.16. Dashed lines indicate the unit cells of the superlattice structure and the arrows indicate directions of adsorbate-substrate forces. (c) and (f) show $\frac{1}{6}$ of the reciprocal space for the hexagonal heavy-domain-wall phases (a) and (d). The solid circles indicate the peaks observed by LEED and crosses indicates the position of C-phase primary peak.

domain-wall structure from the uniform structure by moving the adsorbate molecules along directions indicated by the short arrows in Fig. 10(b). An analogous relationship can also be demonstrated between Fig. 10(d) and 10(e). In Fig. 10(e) we show an unmodulated uniform spacing (7×7) commensurate structure at density 1.16 which follows the same orientational epitaxy relation [curve (a) in Fig. 5] as the γ phase at higher densities (experimentally the γ phase is only observed at densities greater than 1.18). A hexagonal heavy-domain-wall structure at the same density is shown in Fig. 10(d). These pictures show similar topology to that presented in Figs. 10(a) and 10(b). Actually the structures presented in Figs. 10(b) and 10(e) represent a limiting case where the adsorbate-substrate interaction approaches zero, and the hexagonal heavy-domain-wall structures presented in Figs. 10(a) and 10(d) represent another limiting case where adsorbate-adsorbate interaction approaches zero. In fact, neither limit is realistic for D$_2$ on graphite. A structure which is intermediate between these two limits should be expected.

The lateral modulation in the γ phase can be found by fitting calculated satellite intensities for a given modulation model to measured intensities of the neutron-scattering measurements. For an incommensurate struc-

ture in the limit of weak substrate modulation such a modulation can be described easily in reciprocal space.[23] This occurs because the real-space modulation waves are nearly pure sinusoidal waves. In this case the satellite intensity is expected to depend on two parameters: the longitudinal-to-transverse sound-velocity ratio and the amplitude of the substrate corrugation potential. On the other hand, it is easier to characterize the modulation in real space when the mean lattice of the adsorbate matches a higher-order commensurate structure. In this case the consideration of the modulation can be purely geometric and the assumption of weak modulation is not necessary. The number of parameters used to characterize the modulation can be greatly reduced for a lower-order commensurate structure. It is also possible to describe the modulation in the γ phase in terms of relaxed hexagonal heavy-domain-wall network. However, the characterization of the domain-wall relaxation for a heavy domain wall is not as simple as that for a superheavy domain wall. This is because the heavy domain wall is not a purely compressed wall (unlike the superheavy domain wall) and the relaxation of a heavy domain wall will cause both expansion and shear motion of the adsorbate molecules.

One of the higher-order commensurate structures

which matches the orientation of the γ phase is the (4×4) structure presented in Fig. 10(b). There are seven molecules inside each superlattice unit cell, which is indicated by dashed lines. For the purpose of the calculation, it is more convenient to use the hexagonal basis presented in Fig. 11, which also has seven molecules in each cell. Due to the sixfold rotational symmetry and inversion symmetry the substrate modulation can be characterized by two parameters which are chosen to be ϕ and a as indicated in Fig. 11. The structure factor of the superlattice unit cell is calculated as a function of ϕ and a. The calculated neutron-scattering intensity at the leading edge of a diffraction peak from exfoliated graphite is given by[38]

$$I(h,k) = A \frac{m_{hk} |F_{hk}|^2}{\sin^{3/2}(\theta_{hk})} , \qquad \text{(B1)}$$

where A is a constant depending on the wavelength of the incident neutrons and the geometric structure of the sample, F_{hk} is the structure factor of the 2D lattice, θ_{hk} is the scattering angle, and m_{hk} is the multiplicity factor for a given reflection (h,k). In writing Eq. (B1) both the molecular form factor and the Debye-Waller factor are assumed to be unity. The calculated satellite intensities and the neutron-scattering measurements[6,8] are shown in Table II.

For the uniform structure shown in Fig. 10(b), $a = 3.72$ Å and $\phi = 10.9°$, and all satellites, as expected, have zero intensity. The satellites start to show up when the modulation in the nearest-neighbor distance in the overlayer is put in, and the best agreement between the calculated intensities and those measured by neutron scattering is obtained when the modulation parameters are $a = 3.76$ Å and $\phi = 15.5°$ (satellite 3 is not observable since it is always degenerate with the mean lattice reflection peak 4). The structure corresponding to these parameters is

TABLE II. Calculated diffraction intensities from the structure presented in Fig. 11. I_{calc} is the intensity calculated for the (4×4) modulated structure indicated by the crosses in Fig. 11. $I_{neutron}$ is the intensity measured by neutron scattering cited in Ref. 8. Both intensities are normalized to the intensity of the primary peak marked 4 in Fig. 4(b). The asterisk indicates the intensity which is not measurable due to the degeneracy with the primary peak.

Satellite	$\frac{|\mathbf{Q}|}{(\text{Å}^{-1})}$	I_{calc}	$I_{neutron}$
1	1.27	0.01	0.00
2	1.47	0.05	0.05
3	1.95	0.03	*
5	2.12	0.05	0.05
6	2.66	0.01	0.00
7	2.55	0.00	0.00

shown in Fig. 11 by crosses. The positions of adsorbate molecules corresponding to an unmodulated (4×4) structure and a hexagonal heavy-domain-wall structure are also shown by triangles and hexagons, respectively. As one can see, the structure which produced a best fit to the neutron data is only slightly distorted from an unmodulated (4×4) structure. In contrast to this, the distortion from a hexagonal heavy-domain-wall structure is rather large, supporting the hypothesis that the γ phase is, indeed, a modulated IC phase. The fact that the best-fit structure shown by crosses has a modulation opposite to the expected adsorbate-substrate forces [which would pull the molecules toward the hexagons in Fig. 11, as shown in Fig. 10(b)] is not understood.

In the LEED measurements only diffraction beams corresponding to peaks marked 1, 3, and 4 in Fig. 4(b) are observed. The relative intensities of these peaks are roughly equal at an electron energy of 62 eV. At first glance this seems to be inconsistent with the neutron-diffraction measurements. Analogous to the case dis-
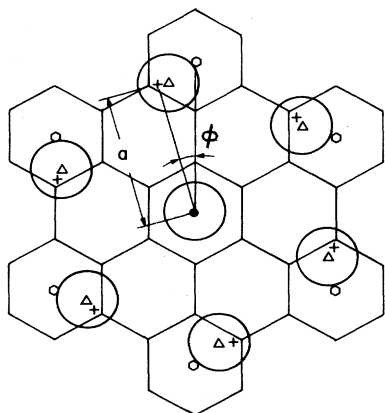

FIG. 11. Modulated structure (indicated by crosses) of the γ phase at $\rho = 1.31$ which produces the best fit to the neutron data. The triangles and hexagons indicate the positions of adsorbate molecules in the uniformly compressed (4×4) triangular structure in Fig. 10(b) and the hexagonal heavy-domain-wall structure in Fig. 10(a). a and ϕ are the parameters which characterize the modulation.
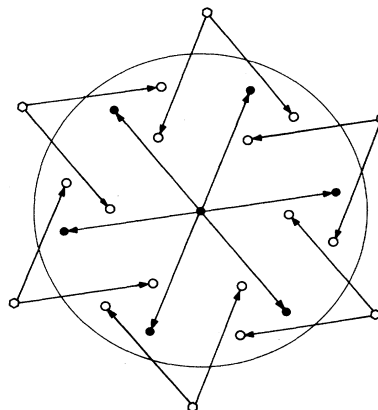

FIG. 12. Positions of double-scattering beams due to the sequential scattering from one rotational domain of the γ phase and graphite. Solid circles indicate the direct-scattering beams and open circles indicate the double-scattering beams.

cussed in Appendix A for the UIC phase, such a discrepancy is primarily caused by the presence of double-scattering beams which are due to sequential scattering from graphite and the overlayer. Figure 12 illustrates the origin of the double-scattering beams from one domain of the γ phase which rotates away from the C-phase direction clockwise by $9.0°$ at a density of 1.25. The single-scattering and double-scattering beams are indicated by solid and open circles, respectively. There is no overlap between "single"-backscattering beams and double-scattering beams, which are shown in Fig. 12. The observed LEED pattern is the sum of the pattern from both positive- (clockwise) and negative- (anticlockwise) rotated domains. The pattern from the negative-rotated domain can be obtained by reflecting that of positive-rotated domain relative to a graphite symmetry direction. For the γ phase LEED peaks from the

negative-rotated domain overlap those from the positive-rotated domain, due to the special rotational epitaxy of the γ phase. For the RIC phase the LEED peaks from positive- and negative-rotated domains are separated. The intensities of the LEED peaks from the RIC phase are approximately equal (within a 30% variation in intensity from one peak to another) at an electron energy near 62 eV. At the same electron energy the intensities of the LEED peaks from the γ are also roughly equal and approximately twice as large as that of the RIC phase. This is consistent with both the γ and the RIC phases being rotated IC triangular phases. This fact also suggests that LEED intensities are dominated by the sequential scattering process. Therefore LEED intensity at the peak marked 1 in Fig. 4(b) can be completely due to the double-scattering beam independent of modulation satellites.

*Present address: Department of Physics, The Pennsylvania State University, University Park, PA 16802.

[1]M. Nielsen, J. D. McTague, and L. Passell, in *Phase Transitions in Surface Films,* edited by J. G. Dash and J. Ruvalds (Plenum, New York, 1980), p. 127.

[2]J. L. Seguin and J. Suzanne, Surf. Sci. **118**, L241 (1982).

[3]F. C. Motteler and J. G. Dash, Phys. Rev. B **31**, 346 (1985); F. C. Motteler, Ph.D. dissertation, University of Washington, Seattle, WA, 1986.

[4]H. Freimuth and H. Wiechert, Surf. Sci. **162**, 432 (1985); **178**, 716 (1986).

[5]H. Freimuth, H. Wiechert, and H. J. Lauter, Surf. Sci. **189/190**, 549 (1987).

[6]H. Wiechert, H. Freimuth, H. P. Schildberg, and H. J. Lauter, Jpn. J. Appl. Phys. **26**, Suppl. 26-3, 351 (1987); H. Wiechert (private communication).

[7]H. P. Schildberg, H. J. Lauter, H. Freimuth, H. Wiechert, and R. Haensel, Jpn. J. Appl. Phys. **26**, Suppl. 26-3, 345 (1987); H. P. Schildberg, Ph.D. dissertation, Christian-Albrechts-Universität, Kiel, Federal Republic of Germany, 1988.

[8]J. Cui, S. C. Fain, Jr., H. Freimuth, H. Wiechert, H. P. Schildberg, and H. J. Lauter, Phys. Rev. Lett. **60**, 1848 (1988).

[9]J. Cui and S. C. Fain, Jr., Bull. Am. Phys. Soc. **31**, 376 (1986); J. Vac. Sci. Technol. A **5**, 710 (1987); Bull. Am. Phys. Soc. **32**, 466 (1987).

[10]X.-Z. Ni and L. W. Bruch, Phys. Rev. B **33**, 4584 (1986).

[11]E. D. Specht, A. Mak, C. Peters, M. Sutton, R. J. Birgeneau, K. L. d'Amico, D. E. Moncton, S. E. Nagler, and P. M. Horn, Z. Phys. B **69**, 347 (1987).

[12]K. Kern, Phys. Rev. B **35**, 8265 (1987).

[13]I. F. Silvera, Rev. Mod. Phys. **52**, 393 (1980).

[14]M. Schick, in *Phase Transitions in Surface Films,* edited by J. G. Dash and J. Ruvalds (Plenum, New York, 1980), p. 65.

[15]N. D. Shrimpton, B. Bergersen, and B. Joos, Phys. Rev. B **34**, 7334 (1986); N. D. Shrimpton, B. Joss, and B. Bergersen, *ibid.* **38**, 2124 (1988).

[16]Ph. Avouris, D. Schmeisser, and J. E. Demuth, Phys. Rev. Lett. **48**, 199 (1982).

[17]S. Andersson and J. Harris, Phys. Rev. Lett. **48**, 545 (1982).

[18]R. E. Palmer and R. F. Willis, Surf. Sci. **179**, L1 (1987).

[19]M. F. Toney, R. D. Diehl, and S. C. Fain, Jr., Phys. Rev. B **27**,

6413 (1983).

[20]J. Cui, Ph.D. thesis, University of Washington, Seattle, WA, 1988.

[21]C. Benvenuti, R. S. Calder, and G. Passardi, J. Vac. Sci. Technol. **13**, 1172 (1976); P. M. Ferm, S. R. Kurtz, K. A. Pearlstine, and G. M. McClelland, Phys. Rev. Lett. **58**, 2602 (1987).

[22]We thank J. Osen for initially developing the system for use with a Vidicon camera and V. L. Eden for adapting it to a charge-coupled-device (CCD) camera.

[23]A. D. Novaco and J. P. McTague, Phys. Rev. Lett. **38**, 1286 (1977); J. P. McTague and A. D. Novaco, Phys. Rev. B **19**, 5299 (1979).

[24]M. Nielsen, J. Als-Nielsen, and J. P. McTague, in *Ordering in Two Dimensions,* edited by S. Sinha (Elsevier, New York, 1980), p. 135. The hexagonal domain-wall structure with $\delta a/a = \frac{1}{3}$ is identical with a hexagonal heavy-domain-wall structure.

[25]The coverage scale used in describing heat-capacity and neutron-diffraction results in Refs. 4–6 is 3.3% higher than the real IC density for D₂ (Ref. 8) and 2–3 % higher for H₂ (Ref. 5).

[26]V. L. Pokrovskii and A. L. Talapov, Phys. Rev. Lett. **42**, 65 (1979).

[27]P. Bak, D. Mukamel, J. Villain, and K. Wentowska, Phys. Rev. B **19**, 1610 (1979).

[28]J. Villain, Surf. Sci. **97**, 219 (1980).

[29]R. D. Diehl and S. C. Fain, Jr., Surf. Sci. **125**, 116 (1983).

[30]J. Talbot, D. J. Tildesley, and W. A. Steele, Surf. Sci. **169**, 71 (1986); B. Kuchta and R. D. Etters, Phys. Rev. B **36**, 3407 (1987).

[31]Normal H₂ and D₂ gases at room temperature consist of 75% odd-J molecules for H₂ and 33% odd-J molecules for D₂ (see Ref. 13).

[32]P. R. Kubik, W. N. Hardy, and H. Glattli, Can. J. Phys. **63**, 605 (1985); P. R. Kubik, Ph.D. thesis, University of British Columbia, Vancouver, B.C., 1984.

[33]Shigeo Hayashi and Kozo Kuchitsu, J. Phys. Soc. Jpn. **42**, 1319 (1977).

[34]N. J. Wu and A. Ignatiev, Phys. Rev. B **25**, 2983 (1982); J. J. Lander, J. Appl. Phys. **35**, 3593 (1964).

[35]C. G. Shaw, S. C. Fain, Jr., and M. D. Chinn, Phys. Rev. Lett. **42**, 65 (1979).

[36]P. W. Stephens, P. A. Heiney, R. J. Birgeneau, P. M. Horn, D. E. Moncton, and G. S. Brown, Phys. Rev. B **29**, 3512 (1984).

[37]S. Calisti and J. Suzanne, Surf. Sci. **105**, L255 (1981); S. Calisti, J. A. Venables, and J. Suzanne, *ibid*. **115**, 455 (1982).

[38]H. Taub, K. Carniero, J. K. Kjems, L. Passell, and J. P. McTague, Phys. Rev. B **16**, 4551 (1977).

[39]C. Tiby, H. Wiechert, and H. J. Lauter, Surf. Sci. **119**, 21 (1982).

[40]A. D. Novaco (private communication); Phys. Rev. Lett. **60**, 2058 (1988).

[41]H. Shiba, J. Phys. Soc. Jpn. **48**, 211 (1980).

[42]K. L. d'Amico, D. E. Moncton, E. D. Specht, R. J. Birgeneau, S. E. Nagler, and P. M. Horn, Phys. Rev. Lett. **53**, 2250 (1984).

[43]C. G. Shaw and S. C. Fain, Jr., Surf. Sci. **83**, 1 (1979).

[44]M. F. Toney and S. C. Fain, Jr., Phys. Rev. B **36**, 1248 (1987); M. F. Toney, Ph.D. thesis, University of Washington, Seattle, WA, 1983.

[45]R. J. Birgeneau, and P. M. Horn, Science **232**, 329 (1986).

[46]J. Suzanne, J. M. Gay, and R. Wang, Surf. Sci. **162**, 439 (1985).

[47]J. M. Kosterlitz and D. J. Thouless, J. Phys. C **6**, 1181 (1973).

[48]B. I. Halperin and D. R. Nelson, Phys. Rev. Lett. **41**, 121 (1978); D. R. Nelson and B. I. Halperin, Phys. Rev. B **19**, 2456 (1979).

[49]A. P. Young, Phys. Rev. B **19**, 1855 (1979).

[50]S. Fain, Jr. and H. You, in *The Structure of Surfaces,* Vol. 2 of *Springer Series in Surface Sciences,* edited by M. A. Van Hove and S. Y. Tong (Springer-Verlag, Berlin, 1985), p. 413.

[51]M. B. Gordon and F. Lançon, J. Phys. C **18**, 3929 (1985).

[52]S. N. Coppersmith, D. S. Fisher, B. I. Halperin, P. A. Lee, and W. F. Brinkman, Phys. Rev. B **25**, 349 (1982).

[53]S. G. J. Mochrie, A. R. Kortan, R. J. Birgeneau, and P. M. Horn, Phys. Rev. Lett. **53**, 985 (1984).

[54]S. G. J. Mochrie, A. R. Kortan, R. J. Birgeneau, and P. M. Horn, Z. Phys. B **62**, 79 (1985).

[55]The first use of the term "hexagonal heavy (domain) wall" to describe this structure was by M. Kardar and A. N. Berker, Phys. Rev. Lett. **48**, 1552 (1982).
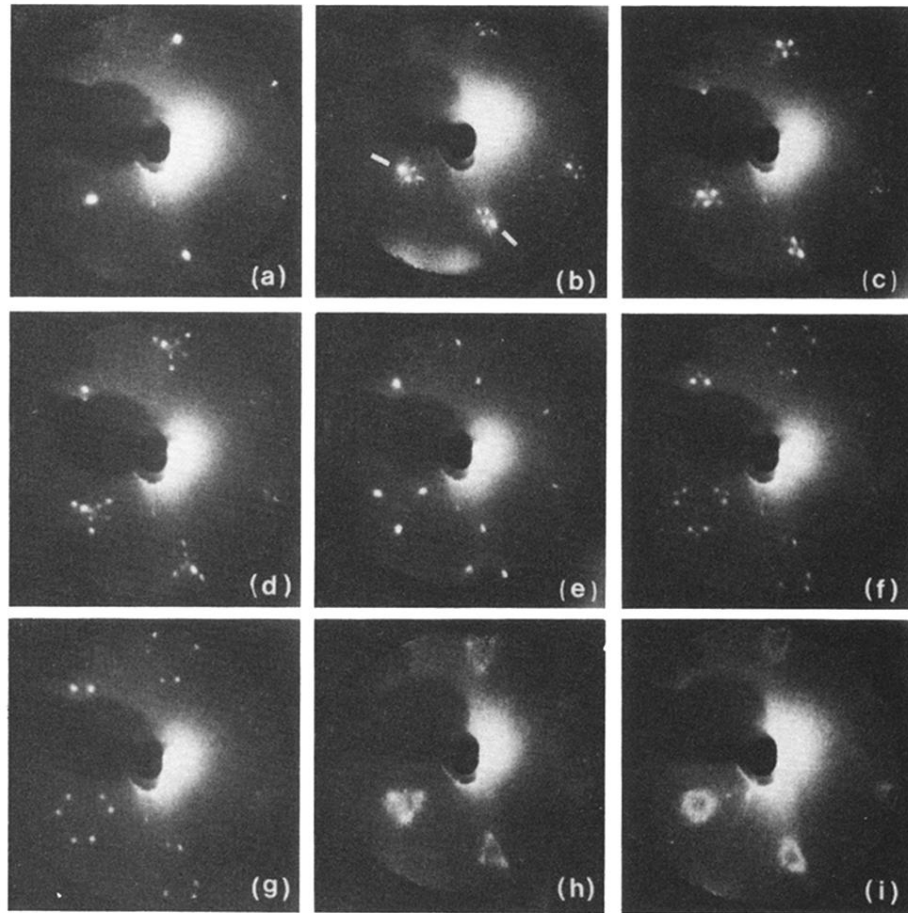
FIG. 1. LEED photographs taken at electron energy 62 eV. The electrons were incident slightly off normal from the Kish-graphite crystal; the angle in (b) is slightly different from the other figures. Due to asymmetric nucleation, the α spots in (b) and (d) are more intense for one of the three possible directions of compression [marked by lines in (b)]. (a) C phase of D_2 at 5 K. (b) α phase of H_2 at 5 K; $\rho = 1.13$. (c) α phase of D_2 at 5 K; $\rho = 1.12$. (d) Coexistence of the α and the γ phase of D_2 at 5 K; $\rho = 1.14$ for the α phase and 1.18 for the γ phase. (e) γ phase of D_2 at 5 K; $\rho = 1.27$. (f) Coexistence of the γ phase and RIC phase of D_2 at 5 K; $\rho = 1.31$ for the γ phase and 1.33 for the RIC phase. (g) RIC phase of D_2 at 5 K; $\rho = 1.36$. (h) β phase of D_2 at 10 K; $\rho = 1.15$. (i) β phase of HD at 10 K; $\rho = 1.18$.